

## Cascade-model analysis of collective motion in relativistic nuclear reactions

Y. Kitazoe\*

*Nuclear Science Division, Lawrence Berkeley Laboratory, University of California, Berkeley, California 94720*

M. Sano

*Institute of Nuclear Study, University of Tokyo, Midoricho, Tanashi, Tokyo 188, Japan*

Y. Yamamura

*Department of Applied Physics, Okayama College of Science, Ridaicho, Okayama 700, Japan*

H. Furutani and K. Yamamoto

*Department of Medical Information, Kochi Medical School, Okoho, Nankoku, Kochi 781-51, Japan*

(Received 29 August 1983)

A new cascade model has been constructed and applied to high-energy heavy-ion collisions, where the emphasis is placed on a systematic study of nuclear collective motion. The model provides a time-dependent microscopic description of nuclear cascade collisions which takes into account some important aspects of the colliding system. The calculated results agree consistently with the experimental data, which otherwise have been interpreted as evidence for collective motion.

### I. INTRODUCTION

A number of experimental and theoretical works have focused on the problem of the formation of high-density and/or high-temperature nuclear matter, which may be induced by relativistic nuclear collisions. To date, several experimental data have suggested the appearance of the collective motion associated with high-density nuclear matter.<sup>1</sup>

The first suggestion came from the forward suppression of low-energy protons ejected in high-multiplicity events (HME's) of  $E_L = 393$  MeV/nucleon Ne + U collisions.<sup>2</sup> A similar tendency of forward suppression was obtained in HME's of  $E_L = 800$  MeV/nucleon Ne + Pb collisions.<sup>3</sup> It was reported in Ref. 4 that such a suppression could not be reproduced by cascade calculations,<sup>5,6</sup> but might be due to hydrodynamical flow.

The second suggestion was found in two-particle correlation functions measured in  $E_L = 800$  MeV/nucleon C + Pb and Ar + Pb collisions.<sup>7,8</sup> The observed data show that two particles tend to be simultaneously emitted on opposite sides of the azimuth. It was pointed out in Refs. 9 and 10 that this behavior of azimuthal correlation is similar to the feature given by the hydrodynamical "bounceoff" effect.

The third suggestion was based on a possible reason why a particular cascade calculation<sup>11</sup> systematically overestimates the observed values of the negative-pion multiplicity in HME's of Ar + KCl collisions. It was pointed out in Ref. 12 that this discrepancy might be due to a bulk compression effect not present in the cascade model.

The fourth suggestion was conjectured from different shapes between proton and pion energy spectra in HME's

of  $E_L = 800$  MeV/nucleon Ar + KCl collisions.<sup>3</sup> Here, the proton data show the "shoulder-arm" shape. This was interpreted in Ref. 13 as evidence of a radially exploding nuclear flow.

If at least one of these suggestions is true, it would be very exciting and interesting. However, it still seems questionable whether they can ever be explained by any means of cascade calculations based on successive two-body collisions, since the usual cascade models contain a variety of problems in treatments of the Pauli principle, the potential well, the Fermi motion, the pion production, and the nucleon-nucleon scattering mechanism, and finally in the framework itself.

In this paper, we would like to improve the above-mentioned problems and state how these effects are incorporated in the cascade model. We further report the results of our cascade model calculations, which are qualitatively consistent with the existing data of present interest.

We organize this paper as follows. In Sec. II, we summarize the main features of the present cascade model. In Sec. III, our calculated results are compared with previous results and data. In Sec. IV, we discuss some differences between our cascade model and others, and make some concluding remarks. The Appendix gives the detailed procedure of our numerical calculations.

### II. FEATURES OF THE PRESENT CASCADE MODEL

Many cascade codes have been developed to describe relativistic nuclear collisions. They can be classified according to method (framework); the time-independent description<sup>5,14,15</sup> and the time-dependent one.<sup>6,11,16,17</sup> The first method is properly applicable to nuclear collisions with a small cascade density, since the nuclear density has to be

kept constant during the collision time. On the other hand, the second method can describe the development of cascade collisions more dynamically but requires a longer computation time.

The main features of the present code are summarized as follows: (1) It describes a time-dependent microscopic behavior of cascade collisions based on the closest-approach method for the two-body collisions. (2) The two-body collisions are determined by using the proton-proton and proton-neutron data, which are distinguishable from each other. We use the polynomial fits of nucleon-nucleon scattering data.<sup>18</sup> (3) The particles and charges are identified before and updated after collisions. (4) The nucleons are distributed initially as a Fermi gas inside the square-well potential. With the time evolution, they are reflected or refracted at the surface of this potential but can pass through freely in the overlapping region between the two nuclei. The refraction takes place when the kinetic energy of a nucleon exceeds the binding energy (including the Coulomb barrier for the proton). (5) The Pauli principle is taken into account by prohibiting the collision process of two nucleons, if they belong to the same nucleus and are in the bound state, or if one or both of them fall(s) into the bound state after the collisions (the bound state of a nucleon is checked by calculating the relative energy of this nucleon measured from the center-of-mass of the projectile or target). (6) The radii of the projectile and the target, and their center-of-mass velocities, are influenced by the collisions, the reflection, and the refraction. (7) The pions are produced by the spontaneous decays of the  $\Delta$  particles formed by the inelastic scatterings, and assumed not to interact with any other particles (this assumption will be removed in the near future). (8) The relativistic effect is considered in the two-body collisions and the Lorentz transformation with respect to momentum and configuration space. A more detailed procedure of our calculations can be followed in the Appendix.

The only free parameter in the present cascade model is the quantity  $r_0$ , which is related to the initial density ( $\rho_0 = 3/4\pi r_0^3$ ) and size ( $R = r_0 A^{1/3}$ ) of the nucleus and to the Fermi energy [ $E_F = (1/3m)(9/8r_0^3)^{2/3}$ ]. In this paper, we use the average energy ( $\epsilon_F = 0.6E_F$ ) as the Fermi motion, to keep the binding energy per nucleon as  $E_B = 8$  MeV except for the Coulomb barrier. Then, the depth of the potential well is given by  $U = \epsilon_F + E_B$ . Alternatively, it is quite easy to give the momentum distribution for the nucleons in the initial state. In this case, however, some nucleons have to be ejected from the nucleus without any collisions, or the binding energy cannot be kept at 8 MeV. This problem will be discussed in calculations of pion multiplicity.

### III. RESULTS OF CALCULATIONS

#### A. Check of the present cascade model

##### 1. Proton-nucleus collisions

The validity of the present model was checked in the case of  $E_L = 800$  MeV P + KCl collisions. The solid lines of Fig. 1 show the calculated result of the proton inclusive

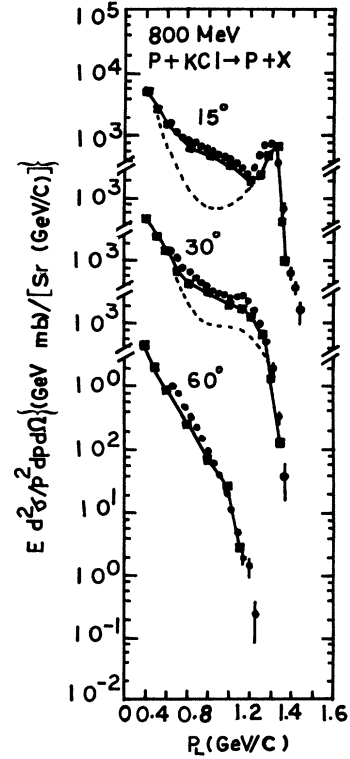


FIG. 1. The proton inclusive cross section in  $E_L = 800$  MeV P + KCl collisions. The solid and the dotted lines show the present results of calculations, which are compared with the experimental data (Ref. 3) (the solid circles). The dotted lines give the elastic scattering part only.

cross section which is compared with the observed data (the solid circles).<sup>3</sup> The dotted lines give only the elastic scattering part without any formation of the  $\Delta$  particles. The inelastic scatterings are appreciable in the intermediate energy region ( $P_L = 0.4 \sim 1.2$  GeV/c) of the energy spectra at forward angles, where the single collisions are predominant. At large angles, the effect of these scatter-

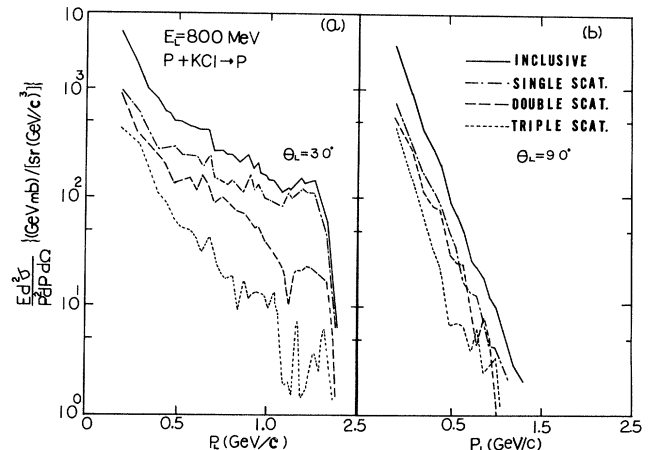


FIG. 2. The calculated respective components of multiple collisions (the single, the double, and the triple collisions) in  $E_L = 800$  MeV P + KCl collisions.

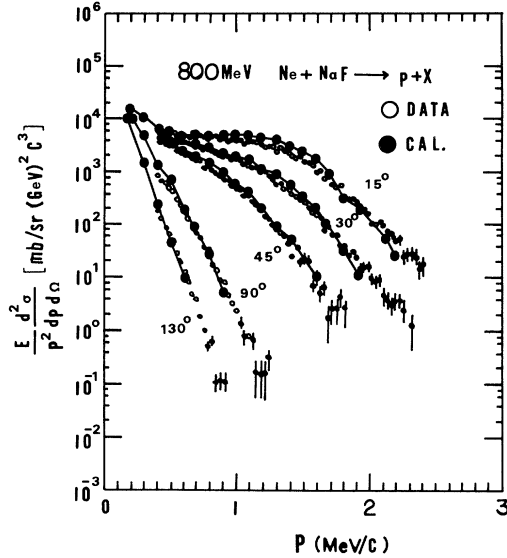


FIG. 3. The proton inclusive cross section in  $E_L=800$  MeV/nucleon Ne + Ne collisions, where the solid and the open circles are the present calculated result and the data (Ref. 19), respectively.

ings is negligible and multiple collisions gradually become important (see Fig. 2). The backward scatterings increase with a decrease of  $r_0$ , which means an increase of the Fermi energy. We fixed  $r_0=1.18$  fm so as to fit the experimental data at  $\theta_L=120^\circ$  (see Fig. 12).

## 2. Nucleus-nucleus collisions

After checking the proton-nucleus collisions, we calculated the proton inclusive cross sections of (a) identical nucleus-nucleus collisions and (b) light-heavy nucleus col-

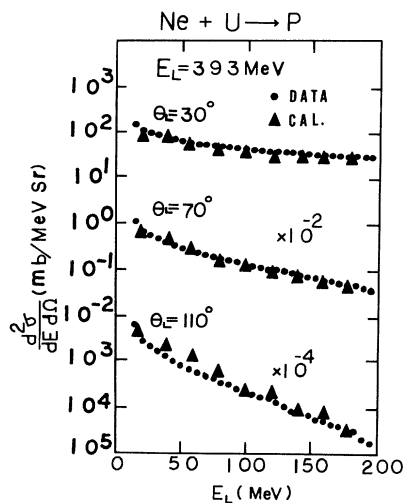


FIG. 4. The proton inclusive cross section in  $E_L=393$  MeV/nucleon Ne + U collisions, where the triangles and the circles represent the present calculated result and the data (Ref. 20), respectively.

lisions, without introducing any additional free parameters. The calculated results are satisfactory, as seen from the two cases  $E_L=800$  MeV/nucleon Ne + Ne (Fig. 3),<sup>19</sup> and  $E_L=393$  MeV/nucleon Ne + U collisions (Fig. 4).<sup>20</sup>

### B. Forward suppression of low-energy protons in $E_L=393$ MeV/nucleon Ne + U central collisions

Let us now discuss the low-energy proton data (the dashed lines of Fig. 5) in HME's of  $E_L=393$  MeV/nucleon Ne + U collisions.<sup>2</sup> These data are suppressed at forward angles, while usual cascade calculations<sup>5,6</sup> give strong forward peakings. The solid squares of Fig. 5 are the calculated result based on Ref. 6. Stöcker *et al.*<sup>4</sup> pointed out that the observed data may be explained by the nuclear fluid-dynamical approach. They also argued the necessity of more realistic treatments of nuclear collisions, as in the classical equations-of-motion approach,<sup>21-23</sup> to confirm the existence of the collective motion.

However, the present cascade calculations (the circles and triangles of Fig. 5) yield much better agreement with the data than the previous calculations.<sup>5,6</sup> Especially the low-energy proton spectrum (the circles) with  $P_L=200$  MeV/c gives a large forward suppression. This comes from the Coulomb effect. Therefore, the neutron spectrum (the circles of Fig. 6) with the same momentum shows a forward peaking. Such an importance of the Coulomb effect was also pointed out in Ref. 24. The calculated proton spectrum (the triangles of Fig. 5) with  $P_L=300$  MeV/c is less isotropic than the data, though it is much more isotropic than the results given by the previous calculations<sup>5,6</sup> (the solid squares). However, it is interesting to see that the calculated neutron spectrum (the triangles of Fig. 6) is quite similar to the recently observed neutron data<sup>25</sup> (the dotted line, in an arbitrary unit) in  $E_L=390$  MeV/nucleon Ne + Pb central collisions. Such a difference between proton and neutron spectra should be discussed after a more precise measurement of the proton spectra. The open triangles in Figs. 5 and 6 show the calculated results without the Pauli blocking effect, which leads to rather higher forward peakings. Finally, the cas-

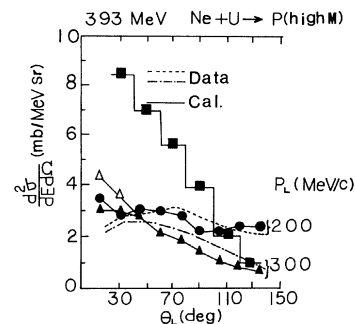


FIG. 5. The calculated low-energy proton spectra and the experimental data (Ref. 2) in high-multiplicity events of  $E_L=393$  MeV/nucleon Ne + U collisions. The circles and the triangles are the present calculated results, while the squares are the calculated result based on Ref. 6. The open triangles are results from neglecting the Pauli blocking effect.

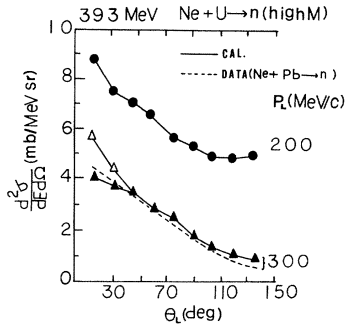


FIG. 6. The calculated low-energy neutron spectra (the solid lines) in  $E_L=393$  MeV/nucleon Ne + U central collisions and the experimental neutron data (Ref. 25) (the dotted line) in high-multiplicity events of  $E_L=390$  MeV/nucleon Ne + Pb collisions. The open triangles are results from neglecting the Pauli blocking effect.

cade density increases with a decrease of the impact parameter, which leads to more and more isotropic scatterings. This tendency of the cascade model is consistent with the data of Ref. 6.

### C. Two-particle correlations and azimuthal-angle dependence

The two-proton correlation functions were measured in  $E_L=800$  MeV/nucleon C + Pb and Ar + Pb collisions by Tanihata *et al.*<sup>7,8</sup> They reported that when a first fast proton is detected at some azimuthal angle, then a second fast proton tends to be emitted on the same side of the azimuth, while a second slow proton is emitted on the opposite side. It was pointed out<sup>1,9,10</sup> that this feature is exactly what is expected from the bounceoff effect of the hydrodynamical flow.

To examine the validity of this speculation, we simulated the azimuthal-angle dependence of ejected protons by

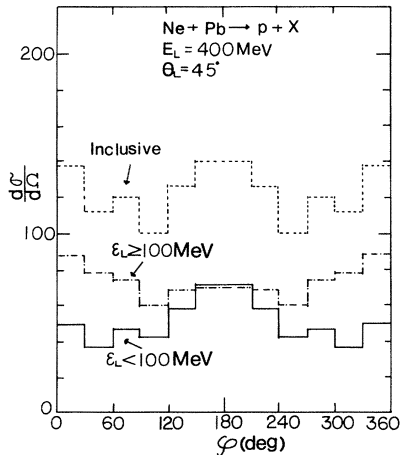


FIG. 7. The azimuthal-angle dependence of ejected protons ( $\theta=45^\circ$ ) in  $E_L=400$  MeV/nucleon Ne + Pb collisions, where  $\psi=0$  is the beam direction in the  $x$ - $y$  plane. Here, the high-energy part ( $\epsilon_L \geq 100$  MeV) shows a bottom around  $\psi=180^\circ$ , while the low-energy part shows a peaking around  $\psi=180^\circ$ . This means the “shadowing” effect.

using our cascade code. In this way, it becomes quite easy to understand the development of cascade collisions in the  $x$ - $y$  plane perpendicular to the beam direction (the  $z$  axis). Figure 7 shows the calculated result in  $E_L=400$  MeV/nucleon Ne + Pb collisions, where the high-energy part ( $\epsilon_L > 100$  MeV) yields a bottom around  $\psi=180^\circ$ , while the low-energy part ( $\epsilon_L \leq 100$  MeV) yields a peak around this angle. This feature is quite consistent with that of the experimental data,<sup>7,8</sup> and becomes more remarkable in peripheral collisions only.

The peripheral-collision process may be divided into two stages, from the viewpoint of the cascade model: The first stage describes the cascade collisions in the overlapping region between the projectile and target; the second stage describes the cascade development toward the remaining regions of these nuclei.

### D. Pion multiplicity in Ar + KCl central collisions

The incident-energy dependence of negative-pion multiplicity was measured in HME’s of Ar + KCl collisions.<sup>12</sup> There appeared a systematic discrepancy between the results of Cugnon’s cascade calculations (the squares of Fig. 8) and those of the experimental data<sup>12</sup> (the triangles). Stock *et al.*<sup>12</sup> proposed the total pion multiplicity as an observable linked to the high-density stage of collisions and regarded the discrepancy as due to a bulk compression effect not present in the cascade model.

However, the present result (the solid circles of Fig. 8) of the cascade calculations does not deviate a lot from the data, though we neglected the absorption effect of the pions (Cugnon’s result includes this effect). The inclusion of this effect will bring better agreement with the data. The open circles of Fig. 8 are results from using the Fermi distribution in the initial state from  $\epsilon=0$  to  $\epsilon=\epsilon_F$  in place of using the fixed value  $\epsilon=\epsilon_F$ . The pion multiplicity at low energies ( $E_c \simeq 100$  MeV/nucleon) is dependent on the treatment of the Fermi motion, as seen in Fig. 8. The

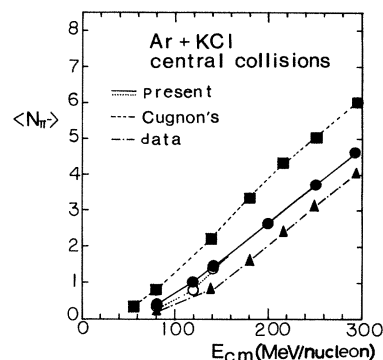


FIG. 8. The negative pion multiplicity in  $E_L=800$  MeV/nucleon Ar + KCl central collisions. The present calculated result (the circles) overestimates the experimental data (Ref. 12), since it neglects the absorption effect of the pion. It, however, is in better agreement with the data than Cugnon’s result (including the absorption effect). The open circles take into account the Fermi distribution in place of using the average value ( $\epsilon_F=0.6E_F$ ), which yields the solid circles. This effect of the Fermi distribution is appreciable at low energies only.

pion absorption is not appreciable at these low energies, since there we have very soft collisions only.

#### IV. DISCUSSION

We have shown in this paper that the calculated results of our cascade model are qualitatively in systematic agreement with the experimental data, which have been interpreted as indications of collective motion. The essential improvement over previous models is the time-dependent description which includes the potential-well effect. Here, we have taken into account (1) the mutual collisions between cascading particles, (2) the reflection and refraction, (3) the isospin effect, (4) the Pauli principle, and (5) the moving radius [ $R_I(t)$ ] and the moving center-of-mass velocity [ $\vec{V}_I(t)$ ], where  $I$  denotes the projectile or target fragment.

Let us discuss some differences between our results and the previous ones.

(1) Figure 9 shows the impact-parameter dependence of proton multiplicity in  $E_L = 800$  MeV/nucleon Ar + Ar collisions. Our result (the solid line) gives smaller values of this multiplicity than the fireball model (the dotted line) in central collisions, but larger values than it in peripheral collisions. On the other hand, Cugnon's result (the dash-dotted line) underestimates the fireball model systematically. This comes mainly from a lack of the potential well (reflection), since nucleons diffuse outside of nuclei without any collisions between them and this diffusion leads to less nuclear density, especially in surface regions of the nuclei. The nuclear binding effect due to the potential well induces a strong cascade development toward the radial direction of the  $x$ - $y$  plane perpendicular to the beam axis. This cascade development in peripheral collisions is very important in explaining the "shadowing" effect which is characteristic of the experimental data<sup>7,8</sup> of two-particle correlations.

(2) The moving center-of-mass effect of the projectile and the target fragment brings a behavior quite similar to

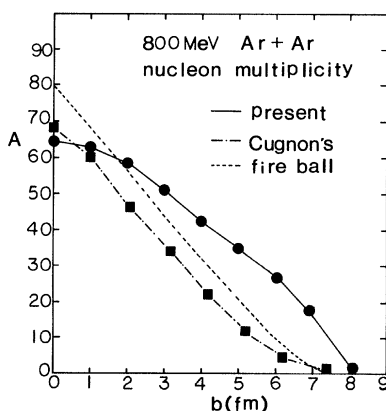


FIG. 9. The impact-parameter dependence of nucleon multiplicity in  $E_L = 800$  MeV/nucleon Ar + Ar collisions. The present calculated result (the solid circles) gives smaller values than the fireball model in central collisions and larger values in peripheral collisions, while Cugnon's result (Ref. 11) (the squares) underestimates the fireball model systematically.

the hydrodynamical "bounceoff" effect.<sup>9,10</sup> Figure 10 shows the impact-parameter dependence of scattering angles for the projectile fragments in  $E_L = 400$  MeV/nucleon Ne + U and Ca + Ca collisions. The projectile fragments in light-heavy nucleus collisions are scattered at much larger angles than those in identical nucleus collisions. This feature is consistent with the experimental tendency.<sup>7,8</sup> It is here noted that the fluctuation of scattering angles becomes very large in the case of central collisions.

(3) The previous cascade calculations<sup>5,6</sup> gave steeper forward peakings<sup>2</sup> than the present one in low-energy proton spectra of  $E_L = 393$  MeV/nucleon Ne + U central collisions (see Fig. 5). Such a feature of strong forward peakings is inconsistent with the observed result, and is associated with both a small cascade density at the intermediate stage of the collision process and a small recoil motion of the target fragments. In fact, the calculated recoiled velocity<sup>5</sup> was underestimated by a factor 2 compared with the observed one<sup>26</sup> in  $E_L = 400$  MeV Ne + Pb central collisions.

(4) As easily supposed, the pion production depends on the way that nucleons collide with each other. The usual cascade models included a variety of problems in treatments of the Pauli blocking, the isospin, the nuclear binding, and the center-of-mass recoil of the projectile and the target fragment. In such a stage of study, therefore, it is still premature to connect the overestimated result of pion multiplicity to the compression phenomena pointed out by Stock *et al.*<sup>12</sup> As argued by them, the agreement between the calculated results and the data in proton-nucleus collisions is quite important for a check of a cascade model. However, this check does not necessarily guarantee the validity of this code in nucleus-nucleus collisions, since there is a great difference of reaction mechanism between proton-nucleus and nucleus-nucleus collisions. Cugnon's cascade model is interesting in a full inclusion of mutual collisions between cascading particles. He also took into account the Pauli blocking effect by using the relative kinetic energy between two colliding particles. This method, however, does not prohibit any first peripheral collisions between two nucleons of the projectile and target.

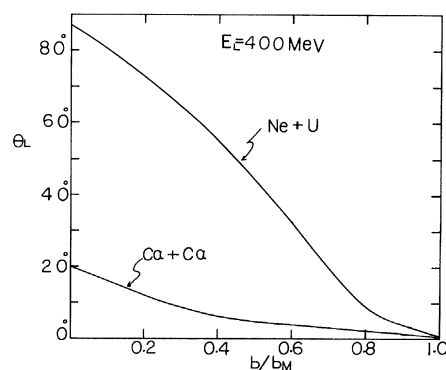


FIG. 10. The impact-parameter dependence of scattering angles of the projectile fragments in  $E_L = 400$  MeV/nucleon Ne + U and Ca + Ca collisions. The scattering angles in light-heavy nucleus collisions are much larger than those in identical-nucleus collisions.

A main problem of our cascade model exists in no absorption of pions, which leads to an overestimation of the pion multiplicity. In proton-nucleus collisions, the amount of this overestimation becomes more serious with an increase of the target mass number. However, we can get good agreement with the experimental data of light nuclei such as Be and C. It is argued here that our model does not underestimate the pion multiplicity in proton-nucleus collisions. In spite of that, our calculated result in Ar + KCl central collisions is in closer agreement with the data than Cugnon's result (see Fig. 8).

As seen in proton-nucleus collisions (Fig. 1), the inelastic scatterings are appreciable at forward angles only. This tendency does not change in Ne + Ne collisions (Fig. 3). The inelastic scatterings take place within the first few collisions between projectile nucleons and target ones. The possibility of these scatterings decreases rapidly with an increase in multiple collisions. After the multiple collisions, we could expect a thermal equilibrium state and/or the nuclear compression. However, Fig. 11 shows that the angular distribution of ejected protons is anisotropic even in the low-energy part ( $\epsilon_c \leq 100$  MeV) of  $E_L = 400$  MeV/nucleons Ar + Ar central collisions. This tendency of anisotropy does not change even if we remove the "corona" effect, which is mainly caused by the single and double collisions. In these respects, it seems very difficult to expect collective motion in identical-nucleus collisions of mass number 40, and to regard the pion multiplicity as a crucial clue to the compression phenomena, since the pions are created mainly at an early stage of the collision process.

Let us discuss here the problem of why the energy spectra of protons, pions, and kaons have different shapes. Recently, Nagamiya<sup>27</sup> tried to explain these different shapes from the viewpoint of a mean-free path: Pions may be rescattered more frequently than protons and especially kaons. Thus, pions are apt to remain inside of nu-

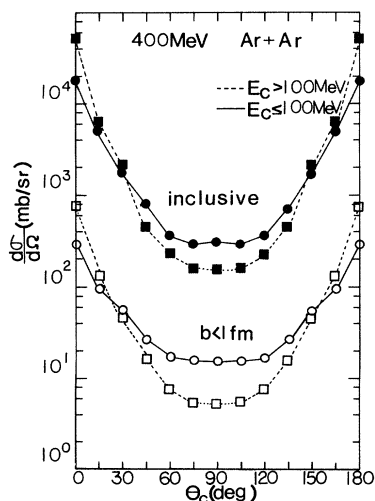


FIG. 11. The proton angular distributions in  $E_L = 400$  MeV/nucleon Ar + Ar collisions. The angular distribution is anisotropic even in the low-energy part ( $E_c \leq 100$  MeV) of the central collisions.

clei and may participate in the collision process until the final stage, while a part of the nucleons and almost all of the kaons may be ejected at early stages of the collision process.

From the viewpoint of the cascade model, however, it is also easy to understand qualitatively why the energy spectra of the pions are steeper than those of the protons, if the pions are produced only through the  $\Delta$  particles. These pions must show primarily the backward and forward peakings in the c.m. frame of two nucleons. This leads to less sideward ejections of pions. On the other hand, the angular distribution of kaons may be rather isotropic in the c.m. frame of two nucleons. In fact, the experimental data<sup>28</sup> show that the sideward kaon spectrum in P + KCl collisions is quite similar, in the equivelocity system, to that in Ar + KCl collisions. It should be noted that the elementary process of kaon production in nucleon-nucleon collisions is very different from that of pion production. This may cause a direct difference in slope between pions and kaons, though the rescattering effect of pions may be much larger than that of kaons.

In this way, we have to find some reaction process which can never be explained by any means of the usual cascade model in terms of the two-body successive collisions. It is here very interesting to investigate the backward emission of energetic protons in proton-nucleus collisions.<sup>29-31</sup> Figure 12 shows our calculated result (the

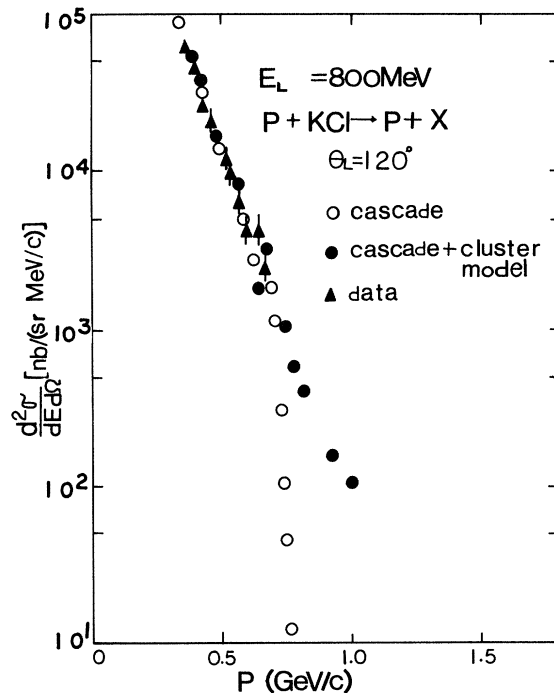


FIG. 12. The proton energy spectra in  $E_L = 800$  MeV P + KCl collisions at  $\theta_L = 120^\circ$ . The usual cascade model (the open circles) in terms of the two-body successive collisions shows good agreement with the experimental data (Ref. 32) (the triangles) at low energies, but a limitation (steep) at high energies. The inclusion (the solid circles) of the cluster model (Ref. 29) yields a linear extension in the logarithmic scale by one order.

circles), which is compared with the data<sup>32</sup> (the triangles) in  $E_L = 800$  MeV P + KCl collisions. Our usual cascade model (the open circles) yields good agreement with the data at low energies, but steepens at high energies around 0.7 GeV/c. We examined the possibility of the incident proton (which still keeps a kinetic energy of higher than 500 MeV) interacting simultaneously with a cluster of more than two nucleons of the target nucleus. It was found numerically that the probability of two nucleons being in the interaction range of the incident proton is ten percent of that of a single nucleon, and that the probability of three nucleons is one percent of that of the single nucleon. An effect of these short-range interactions was taken into account by assuming isotropic scatterings between the incident proton and the clusters. This assumption is essentially equivalent to the cluster model employed by Fujita.<sup>29</sup> As a result, we confirmed that the calculated proton spectrum (the solid circles of Fig. 12) spreads linearly in logarithmic scale toward a higher energy part by one order. Although the data of Ref. 32 were not measured up to very high energies, we can easily suppose<sup>28,29</sup> that the experiment will yield such a straight line as indicated by our result.

The above-mentioned example is only one step to probe into a more sophisticated reaction mechanism. It is, however, very important that we go ahead step by step from simple and easily understandable events gradually toward more complicated ones. The great efforts which have been made in high-energy heavy-ion studies to date suggest to us this importance.

To conclude this paper, a forthcoming important task is to establish a cascade model which can consistently explain a variety of experimental data without introducing any readjustable parameters. After this establishment, we could find an inevitable discrepancy between the cascade model and the data, if it exists. It may be instructive to see that one of the discrepancies can be found in the "sputtering" phenomena induced by atomic collisions between heavy ions and solid surfaces.<sup>32,33</sup>

## ACKNOWLEDGMENTS

Our thanks go to H. Toki for continuous discussions and financial support for the cascade calculations. We also thank S. Nagamiya and O. Hashimoto for useful discussions and financial support for the calculations. We are grateful to M. Gyulassy, P. Danielewicz, H. Gutbrod, K. Nakai, and H. Stöcker for many valuable discussions. One of us (Y.K.) would like to thank N. Glendenning for his hospitality at Lawrence Berkeley Laboratory. He also acknowledges the financial support of the Japan Ministry of Education, Science, and Culture for his stay at Berkeley. This work was supported by the U.S. Department of Energy under Contract DE-AC03-76SF00098.

## APPENDIX

In this appendix, we describe the procedure of the numerical calculations. A flow summary of the procedure is shown in Fig. 13.

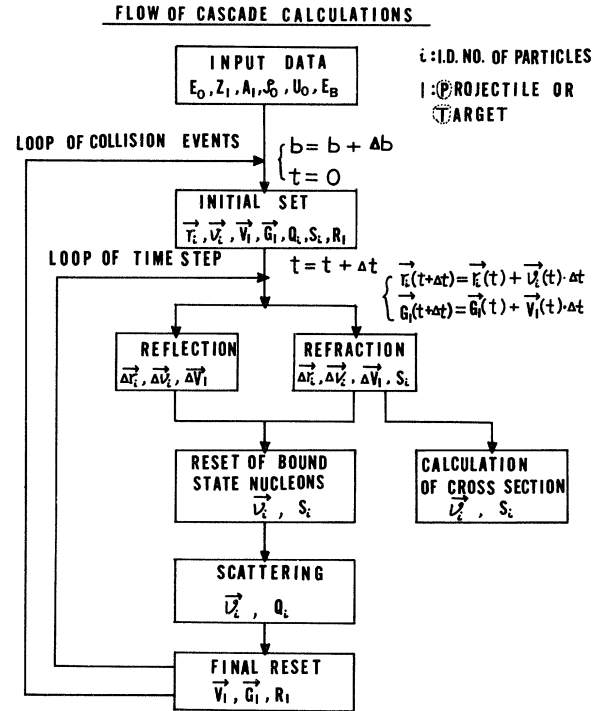


FIG. 13. The flow of the present cascade simulation code. The notations are the following:  $E_L$ —incident energy per nucleon in the laboratory system;  $Z_I$ —charge of the projectile ( $I=P$ ) or target ( $I=T$ );  $A_I$ —mass number of the projectile or target;  $\rho_0$ —normal nuclear density;  $U_0$ —depth of the potential well;  $E_B$ —nuclear binding energy;  $b$ —impact parameter;  $\vec{r}_i$ —position of the  $i$ th particle;  $\vec{v}_i$ —velocity of the  $i$ th particle;  $\vec{V}_I$ —center-of-mass velocity of the projectile or target fragment;  $\vec{G}_I$ —center-of-mass position of the projectile or target fragment;  $R_I$ —radius of the projectile or target fragment;  $Q_i$ —species of the  $i$ th particle ( $Q_i = 1$ , proton,  $Q_i = 2$ , neutron, ...);  $S_i$ —region in which the  $i$ th particle belongs ( $S_i = 2$ , overlapping region between the projectile and target;  $S_i = 1$ , inside of the projectile except for the overlapping region;  $S_i = 3$ , inside of the target except for the overlapping region;  $S_i = 4$ , outside of the projectile and target).

### A. Loop of collision events

#### 1. Initial set

A value of the impact parameter is given. The positions and the velocities of nucleons are randomly distributed in the reference frames of the projectile and target center-of-masses (when we use the average value  $\epsilon_F$  as the Fermi motion, the angles of nucleons are distributed over  $4\pi$ ). The obtained  $\vec{r}_i$  and  $\vec{v}_i$  are transformed into the laboratory frame. The species of nucleons, their associations, and their identification numbers are specified (see the notations  $Q_i$  and  $S_i$ ).

#### B. Loop of time sequence

The time development of  $\vec{r}_i(t)$  and  $\vec{v}_i(t)$  are taken in the laboratory frame. In the next time step,

$$\vec{r}_i(t + \Delta t) = \vec{r}_i(t) + \vec{v}_i(t)\Delta t$$

and

$$\vec{G}_i(t + \Delta t) = \vec{G}_i(t) + \vec{V}_i(t)\Delta t,$$

we have the following procedure:

1. *Reflection and refraction.* The values of  $\vec{r}_i(t)$ ,  $\vec{v}_i(t)$ ,  $Q_i$ , and  $S_i$  are checked in the reference frames of the projectile and target center-of-masses. If a nucleon is positioned outside of the projectile or target fragment, it takes a reflection or refraction according to the kinetic energy in the reference frame in which it belongs. Here, the Coulomb barrier is accounted for protons by using Gamov's penetration factor. The momentum and energy conservations are considered between reflected or refracted nucleons and the residual nucleus. The reflection or refraction is usually once or at most twice during each time step whose interval is very small. When two nucleons are reflected or refracted simultaneously, the conservation laws are applied between the center-of-mass of them and the residual nucleus.

2. *Calculations of the cross section.* Once a particle is refracted (pions can go out freely), it goes into the counter of the cross section, where the species of this particle is identified.

3. *Reset of bound-state nucleons.* By the reflection or refraction of the  $i$ th nucleon, the center-of-mass velocity of the residual nucleus is recoiled by  $\Delta\vec{V}_i$ . Therefore, all of the nucleons of this nucleus are shifted by  $\Delta\vec{V}_i/A_i$ , so that the quantity  $\sum_{j(\neq i)} \vec{v}_j$  may be equal to  $\vec{V}_I + \Delta\vec{V}_i$ . Here,  $A_I$  denotes the mass number of the residual nucleus. Such shifting velocities lead to the stopping effect of the projectile fragment and also the recoiled effect of the target fragment. The values of  $S_i$  are reset when nucleons enter or go out of the overlapping region between two nuclei.

4. *Scattering.* The two-body collisions are determined by using the polynomial fits<sup>18</sup> of nucleon-nucleon collision data in the energy range (1~4000 MeV), where the isospin effect is taken into account. Pions are produced by the spontaneous decays of the  $\Delta$  particles, and the absorption and scattering effects of pions are neglected (this problem will be improved in the near future). The species  $Q_i$  of particles are reset after each collision event.

5. *Final set.* After procedures 1~4, the values of  $\vec{V}_I$ ,  $\vec{G}_I$ , and  $R_I$  are recalculated for the use in the next time step. They are determined by using  $\vec{V}_I = \sum_i \vec{v}_i$ ,  $\vec{G}_I = \sum_i \vec{r}_i$ , and  $R_I = r_0 A_I^{1/3}$ , respectively.

### C. Relativistic effect

For the Lorentz transformation, we define the following statement function in the Fortran statement

$$\vec{v}_i = \text{FLV}(\vec{v}_i, \vec{v}_1, n) \quad (\text{A1})$$

and

$$\vec{r}_i = \text{FLR}(\vec{r}_i, \vec{v}_1, n). \quad (\text{A2})$$

The time evolution is made in the laboratory system. In the above equations, the condition ( $n=1$ ) means the Lorentz transformation of the quantity  $\vec{v}_i$  or  $\vec{r}_i$  from the reference frame of  $\vec{v}_1$  to the laboratory frame. On the other hand, the condition ( $n=-1$ ) means the Lorentz transformation of  $\vec{v}_i$  or  $\vec{r}_i$  from the laboratory frame to the reference frame of  $\vec{v}_1$ . Here, the velocity  $\vec{v}_1$  is set equal to  $\vec{v}_j$  in the case of collision between  $i$ th and  $j$ th nucleons, and equal to  $\vec{V}_I$  for the check of the reflection and the refraction. In this way, the Lorentz transformation is considered very simply and automatically.

\*On leave of absence from Kochi Medical School, Okoho, Nankoku, Kochi 781-51, Japan.

<sup>1</sup>S. Nagamiya and M. Gyulassy, in *Advances in Nuclear Physics* (Plenum, New York, to be published).

<sup>2</sup>R. Stock, H. H. Gutbrod, W. G. Meyer, A. M. Poskanzer, A. Sandoval, J. Gosset, C. H. King, Ch. Luker, Nguyen Van Sen, G. D. Westfall, and K. L. Wolf, *Phys. Rev. Lett.* **44**, 1243 (1980).

<sup>3</sup>S. Nagamiya, M.-C. Lemaire, S. Schnetzer, H. Steiner, and I. Tanihata, *Phys. Rev. Lett.* **45**, 602 (1980).

<sup>4</sup>H. Stöcker, C. Riedel, Y. Yariv, L. P. Csernai, G. Buchwald, G. Graebner, J. A. Maruhn, W. Greiner, K. Frankel, M. Gyulassy, B. Schurmann, G. Westfall, J. D. Stevenson, J. R. Nix, and D. Strottman, *Phys. Rev. Lett.* **47**, 1807 (1981).

<sup>5</sup>Y. Yariv and Z. Fraenkel, *Phys. Rev. C* **20**, 2227 (1979).

<sup>6</sup>J. D. Stevenson, *Phys. Rev. Lett.* **41**, 1702 (1968).

<sup>7</sup>I. Tanihata, M.-C. Lemaire, S. Nagamiya, and S. Schnetzer, *Phys. Lett.* **97B**, 363 (1980).

<sup>8</sup>I. Tanihata, S. Nagamiya, S. Schnetzer, and H. Steiner, *Phys. Lett.* **100B**, 121 (1981).

<sup>9</sup>H. Stöcker, J. A. Maruhn, and W. Greiner, *Phys. Rev. Lett.* **44**, 725 (1980).

<sup>10</sup>L. P. Csernai, W. Greiner, H. Stöcker, I. Tanihata, and S. Nagamiya, *Phys. Rev. C* **25**, 2482 (1982).

<sup>11</sup>J. Cugnon, T. Mizutani, and J. Vandermeulen, *Nucl. Phys.* **A352**, 505 (1981).

<sup>12</sup>R. Stock, R. Bock, B. Brockmann, J. W. Harris, A. Sandoval, H. Stroebale, K. L. Wolf, H. G. Pugh, L. S. Schroeder, M. Maier, R. E. Renfordt, A. Dacal, and M. E. Ortiz, *Phys. Rev. Lett.* **49**, 1236 (1982).

<sup>13</sup>P. J. Siemens and J. O. Rasmussen, *Phys. Rev. Lett.* **42**, 844 (1979).

<sup>14</sup>K. K. Gudima and V. D. Toneev, *Yad. Fiz.* **27**, 658 (1978) [*Sov. J. Nucl. Phys.* **27**, 351 (1978)].

<sup>15</sup>H. W. Bertini, R. T. Santoro, and O. W. Hermann, *Phys. Rev. C* **14**, 590 (1976).

<sup>16</sup>J. P. Bondorf, H. T. Feldmeier, S. Garpman, and E. C. Halbert, *Z. Phys.* **279**, 385 (1976).

<sup>17</sup>E. C. Halbert, *Phys. Rev. C* **23**, 295 (1981).

<sup>18</sup>P. C. Thomas and L. Winsberg, University of California Radi-

- ation Laboratory Report UCRL-9042, 1960.
- <sup>19</sup>S. Nagamiya, T. Tanihata, S. Schnetzer, W. Brueckner, L. Anderson, O. Chamberlain, G. Shapiro, and H. Steiner, Proceedings of the International Conference on Nuclear Structure, Tokyo, 1977, *J. Phys. Soc. Jpn.* **44**, 378 (1978).
- <sup>20</sup>S. Sandoval, H. H. Gutbrod, W. G. Meyer, R. Stock, Ch. Lukner, A. M. Poskanzer, G. Gosset, J.-C. Jourdain, C. H. King, G. King, Ch. Lukner, Nguyen Van Sen, G. D. Westfall, and K. L. Wolf, *Phys. Rev. C* **21**, 1321 (1980).
- <sup>21</sup>Y. Kitazoe, M. Sano, and K. Yamamoto, Proceedings of the International Conference on Nuclear Structure, Tokyo, 1977, *J. Phys. Soc. Jpn.* **44**, 386 (1978).
- <sup>22</sup>A. R. Bodmer, C. N. Panos, and A. D. MacKellar, *Phys. Rev. C* **22**, 1025 (1980).
- <sup>23</sup>D. J. E. Calloway, H. Willets, and Y. Yariv, *Nucl. Phys. A* **327**, 250 (1979).
- <sup>24</sup>O. Scholten, H. Kruse, and W. A. Friedman, *Phys. Rev. C* **26**, 1339 (1982).
- <sup>25</sup>R. Madey, J. C. Varga, B. D. Anderson, A. R. Baldwin, R. Cecil, J. W. Watson, and G. D. Westfall, Lawrence Berkeley Laboratory Report LBL-16281, 1983, p. 113; *Bull. Am. Phys. Soc.* **27**, 25 (1982).
- <sup>26</sup>A. I. Warwick, H. H. Weiman, H. H. Gutbrod, M. R. Maier, J. Peter, H. G. Ritter, H. Stelzer, and F. Weik, *Phys. Rev. C* **27**, 1083 (1983).
- <sup>27</sup>S. Nagamiya, *Phys. Rev. Lett.* **49**, 1383 (1982).
- <sup>28</sup>S. Schnetzer, M.-C. Lemaire, R. Lombard, E. Moeller, S. Nagamiya, G. Shapiro, H. Steiner, and I. Tanihata, *Phys. Rev. Lett.* **49**, 989 (1982).
- <sup>29</sup>T. Fujita, *Phys. Rev. Lett.* **39**, 174 (1977).
- <sup>30</sup>R. Werbeck and V. Highland, *Phys. Rev. Lett.* **36**, 642 (1976).
- <sup>31</sup>V. I. Komarov, G. E. Kosarev, H. Muller, D. Netzband, and T. Steiner, *Phys. Lett.* **69B**, 37 (1977).
- <sup>32</sup>Y. Kitazoe, N. Hiraoka, and Y. Yamamura, *Surf. Sci.* **111**, 381 (1981).
- <sup>33</sup>N. Hiraoka, Y. Kitazoe, and Y. Yamamura, *Radiat. Eff. Lett.* **67**, 7 (1981).